ARTICLE OPEN

Check for updates

Single-mode quantum non-Gaussian light from warm atoms

Jaromír Mika[1]✉, Lukáš Lachman[1], Tomáš Lamich[1], Radim Filip[1]✉ and Lukáš Slodička[1]✉

The distributed quantum information processing and hybridization of quantum platforms raises increasing demands on the quality of light-matter interaction and realization of efficient quantum interfaces. This becomes particularly challenging for needed states possessing fundamental quantum non-Gaussian (QNG) aspects. They correspond to paramount resources in most potent applications of quantum technologies. We demonstrate the generation of light with provably QNG features from a warm atomic ensemble in a single-mode regime. The light is generated in a spontaneous four-wave mixing process in the presence of decoherence effects caused by a large atomic thermal motion. Despite its high sensitivity to any excess noise, direct observability of heralded QNG light could be achieved due to a combination of a fast resonant excitation, large spectral bandwidth, and a low absorption loss of resonant photons guaranteed by the source geometry.

npj Quantum Information (2022)8:123 ; https://doi.org/10.1038/s41534-022-00638-9

INTRODUCTION

Nonclassical states of light have provided a paramount resource for pioneering studies of quantum aspects of radiation and demonstrations of quantum paradigmatic phenomena in matter. They allowed successful initial tests of quantum information theory and evolved into a natural carrier of quantum information over long distances. In modern applications of quantum optics, they have developed into an efficient interconnect between various quantum platforms with complementary properties[1] and correspond to an indispensable resource for quantum communication tasks. The generation of nonclassical single photons has since become nearly a rudimentary experimental exercise and it has been achieved with provably strong sub-Poissonian character in a wide range of implementations[2].

However, for the majority of the prospective applications of quantum technologies, a mere nonclassicality cannot provide a boosting resource over the analogous classical approach, but the enhancement must be supplied by the sensitive quantum non-Gaussian (QNG) properties available either as QNG input states or through the controllable nonlinear QNG interactions[3]. By definition, QNG states hallmark intrinsically nonlinear character of the source[4,5] and already serve as an indispensable resources for the nontrivial character of quantum sensing[6,7], and error correction[8–11], dominantly for motional states of trapped ions and microwave radiation in the superconducting circuits. Despite the optical implementations being significantly more challenging, past two decades brought several stimulating proof-of-principle demonstrations of the QNG states from the heralded cavity OPO sources[12–20], and recently also from heralded single-atom source[21], signified by the observation of the negativity of Wigner function[22]. The analysis of optical fields experiencing strong attenuation, where evaluations based on the negativity of the Wigner function fail, has been enabled by the development and implementation of the QNG criteria based on the precise knowledge of the few lowest photon-number probabilities[23–27]. Such states of light can already find applications in quantum communication and interfaces[28,29]. Although the provable QNG properties of single-photon states have been unambiguously demonstrated in several optical platforms with complementary features, the crucial ability to efficiently interact with matter and form together complex interfering quantum systems remains elusive[3,30–33]. Importantly, utilization of QNG light in the interaction with matter requires well-defined degrees of freedom corresponding to ideally a single optical mode, which would enable an efficient excitation of atomic or solid-state transitions.

The generation of QNG light capable of efficient coherent interaction with target atomic systems and with other QNG light fields has been approached using only a few experimental platforms. Intrinsically single-photon emitters, including single-trapped cold atoms or ions, allow for direct observability of genuine QNG properties due to a good isolation from an environment and are working in a provably close-to a single-mode regime, however, typically provide either low photon rates[21] or low photon-detection efficiencies[25]. On the other hand, QNG sources implemented by a heralded generation of states approaching single-photon Fock states in various parametric optical nonlinear processes[3,14,20,23,24,27,34–36] naturally allow for notably higher photon generation efficiencies assisted by directionality of the underlying optical phase matching, however, they typically contribute with many spectral and temporal modes simultaneously. A multimode spectral nature of a free-space SPDC is typically unavoidable and, in addition, its certification by interferometric measurements is in feasible bandwidth regimes extremely challenging. A conventional enhancement of modeness in these systems corresponds to a severe filtration resulting in a small two-photon coupling efficiencies accompanied by a high susceptibility of observability of QNG to residual noise. Despite significant advancements in demonstrations of operation of narrow-band SPDC sources utilizing optical cavities have been demonstrated[37–43], with most recent works approaching a single-mode regime[44], a provable observation of a single-mode QNG light still remains an open challenge[3]. A rapid development in the realization of spontaneous four-wave mixing (SFWM) photon sources with warm atomic vapors over the past decade brought experimentally very feasible demonstrations of a rich variety of spectrally narrow-band and provably nonclassical light with strongly sub-Poissonian and anti-bunched statistics promising natural applicability for interaction with target atomic ensembles and storage in quantum memories due to their spectral compatibility[27,45–55]. However, to unambiguously surpass the

[1]Department of Optics, Palacký University, 17. listopadu 12, 771 46 Olomouc, Czech Republic. ✉email: mika@optics.upol.cz; filip@optics.upol.cz; slodicka@optics.upol.cz

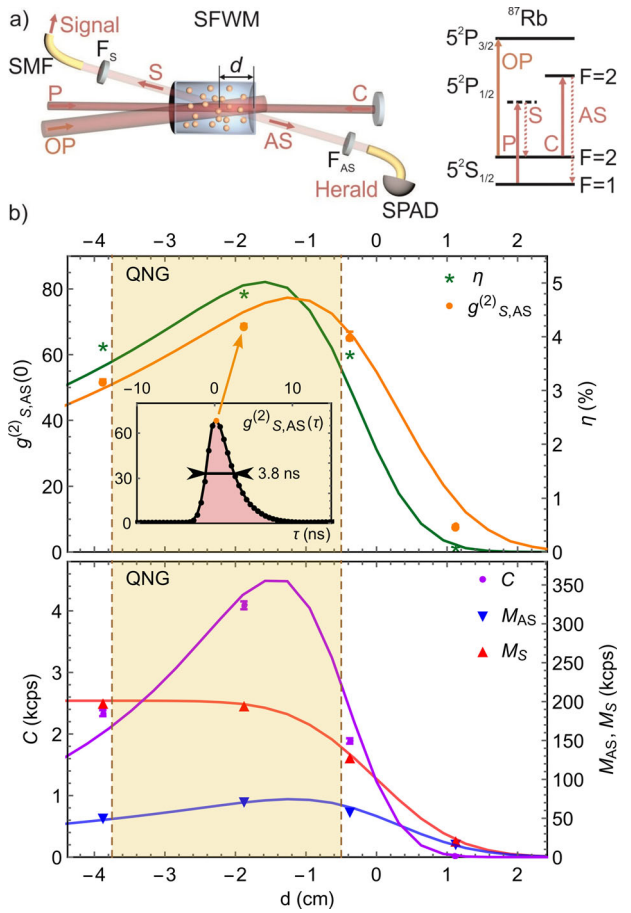

Fig. 1 Scheme of the SFWM source and basic characteristics of generated biphotons. a shows a simplified excitation geometry realized with a single laser frequency with counter-propagating collimated pump (P) and coupling (C) beams. Distance d is defined between the center of the intersection of excitation and observation spatial modes and the cell output viewport along the pump beam propagation direction. The optical pumping (OP) beam effectively covers the interaction area. The Stokes (S) and anti-Stokes (AS) fields are selected by a combination of Fabry–Pérot cavities, Glan–Thompson polarizers, and optical cut-off filters, marked together as F_S and F_{AS}, respectively. Spatial modes are set by the coupling into single-mode fibers (SMF) in two opposite directions. The energy level scheme of ^{87}Rb depicts the SFWM process corresponding to the emission of off-resonant Stokes and near-resonant anti-Stokes fields for the excitation laser set close to the $5S_{1/2}(F=2) \leftrightarrow 5P_{1/2}(F=2)$ transition. The graphs in (**b**) show basic characteristics of generated biphotons including two-photon coupling efficiency η_{2ph} and maxima of the intensity correlation function $g^{(2)}_{S,AS}(0)$ between single-photon avalanche diodes (SPAD) in the heralding—anti-Stokes and in the signal—Stokes channels. The inset shows an example of $g^{2}_{S,AS}(\tau)$. Stokes M_S, anti-Stokes M_{AS}, and coincidence C photodetection rates in kilo-counts/s are shown as red, blue, and magenta data points, respectively. For comparison, QNG marks an area of expectable observability of QNG features. Error bars correspond to a single standard deviation and, where not illustrated, their size is smaller than the size of the corresponding plot symbols.

QNG thresholds[56], the combination of a very low residual two-photon noise component and a high two-photon coupling efficiency, which are partially competing requirements, has to be established at an unprecedented level[3,56]. At the same time, the temporal and spectral modeness of the heralded fields from atomic ensembles with emission spectra dominated by a Doppler broadening in the heralded two-photon regime remains an open question. While the competition between the SFWM gain, absorption losses, and incoherent scattering has been in schemes employing atomic lambda-level configuration widely suppressed with the help of electromagnetically induced transparency for near-resonant anti-Stokes fields, this approach limits feasible spectral bandwidths to several MHz and sets an effective maximal rate of photon generation in the single-mode regime. Another notable approach employs a ladder electronic level scheme, where effects of large Doppler shifts can be conveniently mitigated in a counter-propagating geometry and, in addition, it naturally avoids the dominant noise contribution—Raman noise[27,47,49,54]. We believe, it could present a feasible experimental alternative to the scheme presented here.

Here, we present a demonstration of heralded emission of QNG light from warm atoms in a single optical mode by the generation of photon pairs in a SFWM in a configuration that avoids any additional frequency filtering of the spectrally matched biphotons and, simultaneously, allows for suppression of losses of the near-resonant heralding anti-Stokes field. The measured QNG depth up to 43% of optical loss opens directions to applications in atomic experiments based on this SFWM source.

RESULTS

Spontaneous four-wave mixing in warm atoms

The feasibility of a single-mode QNG regime based on the conditional detection of photonic state from SFWM in a warm atomic ensemble in electronic Λ-like energy level scheme necessitates the suppression of several phenomena contributing with noise and losses to typical realizations of sources of nonclassical light with warm atoms[48,51]. It requires tedious simultaneous optimization of SFWM source parameters. These include the matching of the coherence properties and of the frequency bandwidths, optimization of two-mode nonclassical correlations and two-photon coupling efficiencies, which all have a crucial impact on the feasibility of detection of the challenging QNG states. The presented implementation based on the process of SFWM in a warm ^{87}Rb vapor can benefit from an exclusive feasibility of combination of these properties, while its underlaying fundamental scheme is technically simple and corresponds to a Λ configuration of electronic energy levels with a single counter-propagating laser excitation[51,57]. Figure 1 depicts a simplified experimental scheme and main source characteristics, including the optical filtering setups. We have implemented several crucial improvements of our scheme[55] which contributed to the simultaneous enhancement of the overall two-photon coupling efficiency up to $\eta_{2ph} = P_C/P_{AS} = 9.0 \pm 0.2\%$. Here, P_C and P_{AS} are probabilities of detecting photon coincidence and anti-Stokes single photon within the time window $T_{bin} = 5.67$ ns, respectively. In addition, the generated Stokes M_S and anti-Stokes M_{AS} photon-detection rates were improved by more than tenfold, and a photon coincidence rate was increased twofold. At the same time, sufficiently high nonclassical correlations between Stokes and anti-Stokes fields on the order of $g^{(2)}_{S,AS}(0) \sim 50$, observable for low excitation powers, could be maintained. The combination of the interaction area corresponding to the spatial overlap of excitation lasers and detection mode within the atomic ensemble in the proximity of the vapor cell viewport[55], efficient auxiliary optical pumping (OP) with the help of atomic polarization preserving coating of vapor cell[48], and particular polarization, spectral, and spatial filtering (F_S, F_{AS}), provide conditions for sufficient two-photon coupling efficiencies and, simultaneously, allow for the feasibility of generation of very high nonclassical correlations and low-noise contribution in both Stokes and anti-Stokes fields. Note, that the main purpose of the included broad Fabry–Pérot frequency filters with a full width at half maximum (FWHM) width of about 900 MHz is to suppress any residual laser light and

resonant $5S_{1/2}(F=2) \leftrightarrow 5P_{1/2}(F=2)$ scattering and the SFWM generated Stokes and anti-Stokes signals are transmitted without any significant spectral filtering.

Optimal regime of photon correlations

Photon characteristics and correlations of light generated in the presented SFWM source, including the two-photon coupling efficiency η_{2ph} and $g^2_{S,AS}(0)$ should be theoretically relatively robust with respect to several conventional excitation parameters including atomic temperature, single-photon detuning of the excitation laser, and its optical power. However, in a regime of finite losses and excess noise in the Stokes and anti-Stokes fields, the optimization of $g^2_{S,AS}(0)$ tends to favor a low photon rate due to the random nature of background noise and quadratic scaling of its contribution to false coincidences[58]. This is competing with the practical feasibility of high rate of three-photon-detection events corresponding to the heralding detection on single-photon avalanche photodiode (SPAD) in the anti-Stokes detector and simultaneous multiphoton detection P_{2+} in the Stokes channel with sufficient statistics. In addition, for a given temperature and atomic optical depth, the position of the interaction area has a paramount impact on the absorption losses of anti-Stokes field and on the corresponding source characteristics. Its precise spatial alignment in the proximity of the output viewport of atomic vapor cell allows for the suppression of losses of the heralding near-resonant anti-Stokes field and simultaneously for its broad spectral width. The frequency spectrum of the two-photon correlations gets purified by the attenuation of the resonant scattering and Raman noise in the Stokes channel, where light scattered within the interaction area traverses through the long ensemble of atoms in the same cell. The observed dependence of the source parameters on the spatial position of the interaction region d shown in the Fig. 1b demonstrates the strong effect of the anti-Stokes filtering and corresponding losses on the normalized intensity correlation function $g^{(2)}_{S,AS}(0)$, two-photon coupling efficiency η, and on detectable photon rates. The simulations depicted as solid curves include an independently estimated spatial overlap of atoms with Gaussian excitation and observation optical modes, with the scale of the resulting dependencies of photon-detection rates fitted to Stokes M_S and anti-Stokes M_{AS} data. A detailed description of the employed models and fitting procedures can be found in Supplementary Note 1. The paramount role of the spatial alignment d in a large-bandwidth SFWM source is strongly related to the corresponding possibility of preservation of high nonclassical correlations only on very fast timescales of a few nanoseconds, a limit imposed by decoherence rates of collective excitations of thermal atoms[59]. We note that the observed spatial dependence strongly depends on the interaction length itself, which has been in our case set to a full width at half maximum of 65 ± 7 mm along the excitation direction. We believe that the proximity of the interaction area to the output cell viewport together with a fast excitation regime are crucial for the achievement of QNG properties with SFWM in warm atomic ensembles. Importantly, this approach avoids commonly employed spectral filtering for enhancement of the $g^2_{S,AS}(0)$ and focuses on the suppression of any intrinsic losses and preservation of temporally short nonclassical correlations intrinsic to warm atom systems.

Temporal coherence

The potential of efficient interference and deterministic coherent interaction of light is given by its modeness, which effectively relates to a degree of purity of the quantum state in all of its degrees of freedom. While the polarization and spatial close-to a single-mode operation is in our demonstration elementarily guaranteed by the employment of a high extinction ratio Glan–Thompson polarizers and single-mode optical fibers,

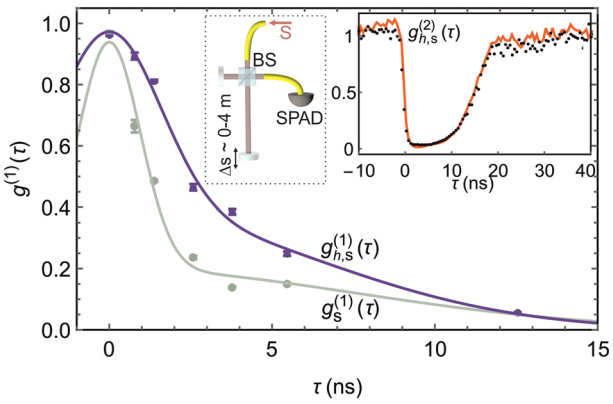

Fig. 2 Measurements of the first degree of coherence $g^{(1)}_S(\tau)$ of Stokes light. The coherence of heralded QNG light $g^{(1)}_{h,S}(\tau)$ and of unconditioned Stokes field is shown as blue and gray plots, respectively. The solid curves correspond to the sum of a two Gaussian functions used for an effective quantitative evaluation of the temporal widths of the measured of $g^{(1)}(\tau)$. The insets show the heralded intensity correlation function $g^{(2)}_{h,S}(\tau)$ evaluated from its direct measurement as black data points and a scheme of Michelson interferometer with a tunable relative path difference Δs covering expectable heralded Stokes temporal wavepackets on the order of ten ns. The measured $g^{(2)}_{h,S}(\tau)$ can be plausibly reproduced by simulation employing the measured $g^{(2)}_{S,AS}(\tau)$ and Stokes intensity profile $I_S(\tau)$ estimated from the $g^{(2)}_S(\tau)$ measurement in an unheralded regime, what suggests a close to unity overlap between the unconditioned and heralded temporal intensity functions of Stokes field. Error bars correspond to a single standard deviation and, where not illustrated, their size is smaller than the size of the corresponding plot symbols.

temporal coherence has to be accessed by additional phase-sensitive interferometric measurements. The measured heralded intensity autocorrelation functions could, in principle, consist of an incoherent mixture of several temporal envelopes corresponding to several spectral components. This is particularly important to study in the case of light generated from warm atomic vapors where a large Doppler broadening results in incoherent spectral widths of more than an order of magnitude larger than natural linewidths of employed transitions of alkali atoms. On the other hand, the observable intensity correlations $g^{(2)}(\tau)_{S,AS}$ already show signatures of intensity profiles much below the lifetime of the employed excited states, which can be attributed to the collective nature of the employed SFWM interaction[60–62].

We characterize the number of contributing spectral and temporal modes of the generated Stokes field by analysis of the first degree of coherence $g^{(1)}_S(\tau)$. The coherence is measured in a Michelson interferometer with up to approximately 4 m path difference which allows for the relative time delays of more than $\tau \sim 12$ ns corresponding to the extent of observed intensity wavepackets. Figure 2 shows first-order coherence functions evaluated from the heralded measurement of the QNG Stokes field $g^{(1)}_{h,S}(\tau)$, and $g^{(1)}_S(\tau)$ evaluated by including all photons detected in the Stokes channel from the same data acquisition. They can be understood by considering spectral properties of the four-wave-mixing and underlying phase matching condition, where the third-order susceptibility $\chi^{(3)}$ determining the biphoton spectral waveform includes the enhancement due to the two-photon resonance[48,61]. Crucially, the coherence of the heralded Stokes field is significantly enhanced compared to the non-heralded case, which can be mostly attributed to the residual electromagnetically induced transparency spectral filtering in the heralding anti-Stokes channel upon passing the atomic ensemble

and the corresponding post-selection of Stokes photons through spectral correlations implied by the phase matching conditions[48]. The exploitations of analogous spectral correlations have been paramount to the design of SPDC photon sources and their applications[63], while they remained largely unexplored in the SFWM domain. A dedicated study of spectral correlation properties in SFWM sources will be part of our next experimental efforts as it reaches beyond the scope of this work. The temporal mode number has been accessed by a quantitative comparison of temporal widths of intensity profiles corresponding to the measured first and second-order correlation functions as $M_t = \tau_1/\tau_2 = 1.43 \pm 0.09$. Here, $\tau_1 = 6.5 \pm 0.2$ and $\tau_2 = 4.5 \pm 0.2$ are mean temporal lengths of the intensity profiles $I_{h,S}(\tau)$ evaluated from the measured $g_S^{(2)}(\tau)$ and $g_{h,S}^{(1)}(\tau)$, respectively. The M_t quantifies the mutual temporal coherence of two light sources with a given intensity and coherence temporal profiles. The estimation of the $I_{h,S}(\tau)$ has been realized indirectly as follows. We used deconvolution of the non-heralded Stokes autocorrelation $g_S^{(2)}(\tau)$ for accessing $I_S(\tau)$ and verified that the following estimation of intensity autocorrelation function of heralded Stokes light $g_{h,S}^{(2)}(\tau) \approx g_S^{(2)}/g_{S,AS}^{(2)}$ gives quantitatively good agreement with the measurement. The measured and simulated $g_{h,S}^{(2)}(\tau)$ shown in the inset of the Fig. 2 give high overlap of 96%, where the residual difference can be partially attributed to the measurement noise. This justifies the consideration of $I_{S,h}(\tau) \sim I_S(\tau)$ for the presented evaluation of an approximate number of modes in the heralded Stokes field. The measured $g_{h,S}^{(1)}(0) = 0.963 \pm 0.004$ and $g_S^{(1)}(0) = 0.971 \pm 0.003$ differ slightly from ideal value, probably due to residual power drifts between the calibration measurements with the coherent laser beam and measurements with Stokes fields.

Quantum non-Gaussian light

We focus on an unambiguous proof of the QNG character of conditionally generated Stokes field and estimation of its temporal envelope. Here we discuss exclusively the configuration with anti-Stokes trigger and Stokes signal field, because strongly off-resonant Stokes field experiences significantly smaller absorption losses and a corresponding enhancement of two-photon coupling efficiency. However, we note that we have successfully observed the QNG features also for the inverted configuration with the signal field corresponding to a near-resonant anti-Stokes emission, with corresponding results presented in Supplementary Note 2. We also expect feasibility of optimization of the absorption parameters simultaneously for both of the two output channels by the employment of the excitation scheme with independent pump and coupling beams[48].

The QNG of the generated photonic states can be proven by the evaluation of criteria based on the estimated photon-number probabilities[23,56,64]. In the presented experiment, they are detected using a combination of fiber-coupled single-photon avalanche photodiodes (SPADs). A single heralding SPAD is employed in the anti-Stokes channel, while a pair of SPADs in the signal-Stokes detection mode is arranged in the single-mode fiber implementation of a Hanbury–Brown–Twiss setup. In the case of the single-photon generation in the presence of noise and losses, the heralded Stokes can be approximately described by

$$\rho \sim P_0|0\rangle\langle 0| + P_1|1\rangle\langle 1| + P_{2+}\left(\sum_{n=2}^{\infty}|n\rangle\langle n|\right). \quad (1)$$

Here P_0 and P_1 correspond to probabilities of vacuum and single-photon states, respectively, and the probability of multiphoton contributions $P_{2+} = 1 - P_0 - P_1$. Importantly, these probabilities provide sufficient knowledge of the photon statistics for the estimation of the QNG properties of light emitted by a single-photon source and, at the same time, can be unambiguously evaluated from photon autocorrelation measurements with single-photon detectors[23–25,27,56,64]. The sufficient condition for proving the QNG properties of the detected states can be then evaluated as[23,64]

$$P_{2+} < \frac{2}{3}P_1^3, \quad (2)$$

which holds for states with $P_{2+} \ll 1$. Note, that this criterion remains reliable also for multimode states of light.

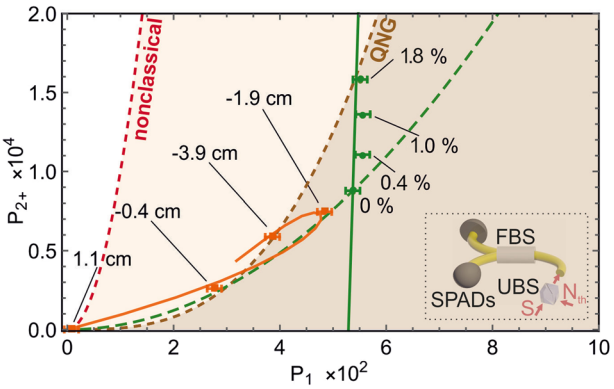

Fig. 3 Measured statistical properties of heralded Stokes light. Observed QNG features are parameterized by photon-number probabilities P_1 and P_{2+} of a single and multiphoton events observed in the Stokes mode, respectively. The orange data points show raw photodetection probabilities with the corresponding simulation depicted by the orange solid curve. The region of observability of QNG properties corresponds to the shaded areas with the dashed thresholds given by the Eq. (2). The QNG is unambiguously proved, despite the large sensitivity of their detectability in the presented feasible range of two-photon coupling efficiencies and corresponding Stokes single-photon probabilities P_1. This sensitivity can be well characterized and quantified by measurement of a QNG depth, which can be accessed by introduction of an excess thermal noise[23,34]. The resulting thermalization trajectory for the interaction position of the interaction area $d = -1.9$ cm is shown as green data points with the excess thermal noise to Stokes signal ratio $NSR_{h,exc} = P_{th,exc}/P_1$ explicitly indicated. The corresponding theoretical model is derived by considering mixing of the generated QNG state with an ideal thermal light. The red dashed curve shows the evaluation of the dependence of the observed QNG features on bare losses in the Stokes mode. The red dashed curve depicts the threshold on the observability of the nonclassical character of measured photon statistics by conventional estimation of the sub-Poissonian value of α parameter. The photon statistics is accessed by detection arrangement consisting of the balanced fiber splitter (FBS) with a fiber-coupled SPAD in each output port shown in the inset. The optional addition of thermal light has been implemented using the unbalanced T:R = 90:10% beamsplitter (UBS). Error bars correspond to a single standard deviation.

The evaluations of QNG features for the presented spatial position characterization are depicted in Fig. 3. The heralded signal-Stokes single-photon generation probability has been accessed as $P_1 = C/M_{AS}$, where C is the total number of coincidences between Stokes and anti-Stokes channels, and M_{AS} is the detected anti-Stokes photon rate. The probability $P_{2+} = 2R_{C,h}/M_{AS}$, where $R_{C,h}$ is the rate of three-coincidences, a situation where both Stokes signal detectors in a HBT configuration and the heralding anti-Stokes detector register a photon within the same time bin[24]. The factor of two accounts for cases where the two photons in HBT arrive at the same detector. The presented probabilities are not compensated for any experimental losses. The coincidence time window has been optimized in steps corresponding to integer multiples of the fundamental resolution of the employed time-tagging device of 81 ps to minimize the value P_{2+}/P_1^3, with resulting optimal value $T_{bin} = 5.67$ ns. Generated photon statistical distributions surpass the criteria (2) for an

interval of the positions of the interaction region d from -5 to -38 mm, with a measured peak value at $d = -19 \pm 2$ mm corresponding unambiguously to the QNG state. The observed trajectory reflects a clear asymmetry of the observable Stokes and anti-Stokes losses with respect to position d, which can be understood by considering a dominant suppression of the heralding efficiency and of the two-photon coupling efficiency for negative and positive values of d, respectively. We analyze the sensitivity of observed QNG features to losses and to excess thermal noise in order to allow for its comparison with other sources and to estimate its feasibility for interactions with target atomic ensembles in the presence of realistic noise contributions. The thermal light with a close to ideal thermal statistics is generated by SFWM process in another atomic cell, where the emission is collected without any conditioning on the anti-Stokes detection. This effectively corresponds to tracing of the anti-Stokes field in the two-mode output of the SFWM and results in close to ideal photon bunching and Bose-Einstein photon-number probability distribution[58]. The realized thermal source emission is single-mode and has a relatively narrow frequency bandwidth of about 77 MHz set to allow for observation of close to the ideal bunching value $g^{(2)}(\tau = 0) = 1.95 \pm 0.03$ observable with a finite timing jitter of the employed SPADs. The depth of the generated QNG states is accessed by the measurement of photon statistics of light resulting from mixing of the generated QNG Stokes field with the thermal light at the T:R = 90:10% unbalanced beamsplitter (UBS). The QNG light is sent to a high transmissivity port to limit its loss. Figure 3 shows the evaluated trajectories for the state generated in the optimal regime of the d-parameter for the case of ideal attenuation and for the case of experimentally emulated thermalization with light with a mean excess thermal photon rate of $N_{\mathrm{th,exc}}$. The corresponding threshold has been reached for an excess noise-to-signal ratio $\mathrm{NSR_{h,exc}} = P_{\mathrm{th,exc}}/P_1 = 0.018 \pm 0.002$, where $P_{\mathrm{th,exc}} = N_{\mathrm{th,exc}} T_{\mathrm{bin}} = (9.8 \pm 0.9) \times 10^{-4}$ is the measured overall probability of thermal photon detection in a given time window, and $P_1 = 0.053 \pm 0.001$ is the single-photon probability in the absence of excess noise. The thermalization threshold on observability of QNG at corresponding P_1 gives an overall limit on the ratio of noise to heralded Stokes signal $\mathrm{NSR_h} = P_{\mathrm{th}}/P_1 = 0.04 \pm 0.01$ and on the corresponding bare ratio of the non-heralded Stokes rate and thermal photon number $\mathrm{NSR_r} = N_{\mathrm{th}}/M_S = 0.83 \pm 0.06$. The simulation of the effect of a linear optical loss in the Stokes channel for the same data point is shown as a green dashed line. It suggests expectable preservation of the QNG observability for up to 43.4% of optical loss. The residual multiphoton contribution $P_{2+} = (8.8 \pm 0.1) \times 10^{-5}$ is partially given by the inevitable thermal noise contributions to the detected Stokes mode coming from the complementary SFWM geometries[58] and by imperfect spatial matching of the coupled Stokes and anti-Stokes modes. The error bars shown for all data points presented in Fig. 3 were evaluated from a set of five consecutive measurements and correspond to a single standard deviation of the evaluated parameters. They thus mostly account for short-term statistical uncertainties and do not include long-term drifts of experimental parameters on timescales of days or repeatability of the spatial alignment, which were estimated independently to about ±0.3% of the absolute value of the heralding efficiency η. This corresponds to the relative fluctuation of the mutual spatial alignment of two fiber-coupled detection channels of 6%, which accounts for a visible shift between the set of green data and the corresponding orange data point at $d = -1.9$ cm with no excess thermal noise. The evaluations of the corresponding bare nonclassical properties of the heralded Stokes field and their behavior in the presence of excess thermal noise can be found in Supplementary Note 3. We remind that, besides the crucial role of estimation of QNG depth as a general and robust comparison of quality of QNG sources with extensions beyond the optical domain[65], it can be also employed for estimation of tolerance of generated QNG properties against intrinsic noise sources and provide a means for an unambiguous optimization of source parameters.

DISCUSSION

The QNG properties of light correspond to a paramount resource in majority of prospective applications of quantum technologies[3,8–11]. At the same time, the ability to form hybrid quantum systems by controllable interactions provably operating between many QNG states is crucial for reaching their practically useful limits. We have demonstrated a broadly applicable and accessible experimental methodology for generation and analysis of single-mode QNG states in SFWM process with warm atoms. We have shown that photon pairs emitted from SFWM process can provide a conditional generation of statistical properties that prove an advanced level of experimental control and, importantly, their temporal coherence properties suggest close-to a single-mode operation. The presented scheme with effectively short warm atomic medium provides a high two-photon coupling efficiency without compromising the amplitude of the nonclassical correlations between anti-Stokes and Stokes fields. At the same time, it allows for high photon rates, a necessary condition for feasibility of observation of QNG of photon fields approaching single-photon Fock states in the presence of any residual noise and for practical applicability of the generated QNG light. We provide a direct comparison of achieved statistical parameters relevant for the evaluation of the feasibility of observation of QNG properties with other sources of nonclassical light based on the SFWM in warm atomic vapors in the Supplementary Discussion. Importantly, the availability of natural thermal light sources based on the same process could be employed for a direct experimental evaluation of thermal depth of generated QNG properties, which further confirmed very low thermal noise contribution in the observed photon statistics of the generated Stokes light field. We remind that we have additionally confirmed that QNG regime is achievable also for the anti-Stokes field, although with a quality and depth significantly compromised by lower two-photon coupling efficiency due to residual absorption of near-resonant photons. We foresee significant enhancements of both heralding and two-photon coupling efficiencies by a bare suppression of the passive optical losses in our experiment, with a feasible two-photon coupling efficiencies of about 32%. The presented generation of photonic single-mode QNG states capable of a storage and controllable interaction with a bandwidth-compatible target atomic systems[66–69] represents a crucial step for realization of distribution of quantum non-Gaussianity and its local or distributed processing. Together with advancements in the realization of high-efficiency and low-noise optical quantum memories[70–73], the presented source parameters promise potential for an on-demand QNG light source. Demonstrated close-to single-mode operation can provide the missing fundamental ingredient for efficient nonlinear interactions with QNG light in atomic ensembles[74–76].

METHODS

Spontaneous four-wave mixing excitation scheme

In the following description of the SFWM experimental setup we focus only on parts which we found to be paramount for generation and observation of the single-mode QNG states. The SFWM is driven by a continuous-wave single-frequency output of a Ti:Saphire laser blue-detuned about $\Delta = 400$ MHz from the $5S_{1/2}(F = 2) \leftrightarrow 5P_{1/2}(F = 2)$ transition. The excitation geometry corresponds to a counter-propagating pump-coupling configuration in a convenient retro-reflection setup. Excitation of atoms prepared in the electronic ground state $|g\rangle = 5S_{1/2}(F = 1)$ results in the excitation-emission

cycles $|g\rangle \rightarrow |a_1\rangle \rightarrow 5S_{1/2}(F=2) \rightarrow 5P_{1/2}(F=2) \rightarrow |g\rangle$, where $|a_1\rangle$ corresponds to a virtual energy level red-detuned from the $5P_{1/2}(F=2)$ by ~6.4 GHz. The temperature of the cell was set to 323 K and excitation beam power was 100 mW for all measurements except where explicitly stated otherwise. We remind that a small-angle scattering geometry with $\alpha_{sc} \sim 1.8 \pm 0.1°$ is crucial for the suppression of decoherence of the collective spin wave due to thermal atomic motion on short timescales[59]. In addition, the Stokes to anti-Stokes correlations are strongly enhanced by the introduction of an auxiliary optical pumping beam set close to the resonance with the $5S_{1/2}(F=2) \leftrightarrow 5P_{3/2}$ transition together with a paraffin coating deposited on the inner surfaces of the vapor cell, which substantially suppress the Raman noise in the anti-Stokes mode[48,50]. The polarization and spatial degrees of freedom of generated photon pairs are defined by the phase matching condition, which, in the implemented standing-wave excitation geometry and double-λ energy level scheme, results in convenient counter-propagating detection directions and identical linear polarizations[51,57]. The polarization and spatial single modeness of Stokes and anti-Stokes fields is guaranteed by the combination of Glan–Thompson polarizer and single-mode optical fibers in each detection channel. The spatial optimization of a coupling to a pair of single-mode optical fibers is optimized to maximize the mutual spatial mode overlap using an auxiliary off-resonant optical beam passing from the Stokes to the anti-Stokes optical fiber, with the resulting overall coupling efficiency matching well independently estimated optical losses of about 79%. The full width of the waist of the observation Gaussian mode at the position of the interaction area, which is defined as an overlap of the observation and excitation optical modes, corresponds to 95 ± 5 μm. Fabry–Pérot filters in both heralding and signal arms have FWHM frequency bandwidth of 900 ± 10 MHz and are tuned to maximize the transmission of the anti-Stokes and Stokes fields, respectively.

DATA AVAILABILITY

The data are available from the authors upon reasonable request.

Received: 10 January 2022; Accepted: 30 September 2022;
Published online: 26 October 2022

REFERENCES

1. Kurizki, G. et al. Quantum technologies with hybrid systems. *Proc. Natl Acad. Sci. USA* **112**, 3866–3873 (2015).
2. Slussarenko, S. & Pryde, G. J. Photonic quantum information processing: a concise review. *Appl. Phys. Rev.* **6**, 041303 (2019).
3. Lvovsky, A. I. et al. Production and applications of non-Gaussian quantum states of light. Preprint at https://arxiv.org/abs/2006.16985 (2020).
4. Hudson, R. L. When is the Wigner quasi-probability density non-negative? *Rep. Math. Phys.* **6**, 249–252 (1974).
5. Walschaers, M. Non-Gaussian quantum states and where to find them. *PRX Quantum* **2**, 030204 (2021).
6. McCormick, K. C. et al. Quantum-enhanced sensing of a single-ion mechanical oscillator. *Nature* **572**, 86–90 (2019).
7. Wolf, F. et al. Motional fock states for quantum-enhanced amplitude and phase measurements with trapped ions. *Nat. Commun.* **10**, 1–8 (2019).
8. Michael, M. H. et al. New class of quantum error-correcting codes for a bosonic mode. *Phys. Rev. X* **6**, 031006 (2016).
9. Hu, L. et al. Quantum error correction and universal gate set operation on a binomial bosonic logical qubit. *Nat. Phys.* **15**, 503–508 (2019).
10. Campagne-Ibarcq, P. et al. Quantum error correction of a qubit encoded in grid states of an oscillator. *Nature* **584**, 368–372 (2020).
11. Flühmann, C. et al. Encoding a qubit in a trapped-ion mechanical oscillator. *Nature* **566**, 513 (2019).
12. Lvovsky, A. I. et al. Quantum state reconstruction of the single-photon fock state. *Phys. Rev. Lett.* **87**, 050402 (2001).
13. Zavatta, A., Viciani, S. & Bellini, M. Tomographic reconstruction of the single-photon fock state by high-frequency homodyne detection. *Phys. Rev. A* **70**, 053821 (2004).
14. Ourjoumtsev, A., Tualle-Brouri, R., Laurat, J. & Grangier, P. Generating optical schrödinger kittens for quantum information processing. *Science* **312**, 83–86 (2006).
15. Ourjoumtsev, A., Tualle-Brouri, R. & Grangier, P. Quantum homodyne tomography of a two-photon fock state. *Phys. Rev. Lett.* **96**, 213601 (2006).
16. Miwa, Y. et al. Exploring a new regime for processing optical qubits: squeezing and unsqueezing single photons. *Phys. Rev. Lett.* **113**, 013601 (2014).
17. Bimbard, E. et al. Homodyne tomography of a single photon retrieved on demand from a cavity-enhanced cold atom memory. *Phys. Rev. Lett.* **112**, 033601 (2014).
18. Le Jeannic, H., Cavaillès, A., Huang, K., Filip, R. & Laurat, J. Slowing quantum decoherence by squeezing in phase space. *Phys. Rev. Lett.* **120**, 073603 (2018).
19. Zapletal, P. et al. Experimental fock-state bunching capability of non-ideal single-photon states. *Optica* **8**, 743–748 (2021).
20. Ra, Y.-S. et al. Non-Gaussian quantum states of a multimode light field. *Nat. Phys.* **16**, 144–147 (2020).
21. Hacker, B. et al. Deterministic creation of entangled atom–light schrödinger-cat states. *Nat. Photonics* **13**, 110–115 (2019).
22. Schleich, W. P. *Quantum Optics in Phase Space* (John Wiley & Sons, 2011).
23. Straka, I. et al. Quantum non-Gaussian depth of single-photon states. *Phys. Rev. Lett.* **113**, 223603 (2014).
24. Ježek, M. et al. Experimental test of the quantum non-Gaussian character of a heralded single-photon state. *Phys. Rev. Lett.* **107**, 213602 (2011).
25. Higginbottom, D. B. et al. Pure single photons from a trapped atom source. *N. J. Phys.* **18**, 093038 (2016).
26. Ježek, M. et al. Experimental test of the strongly nonclassical character of a noisy squeezed single-photon state. *Phys. Rev. A* **86**, 043813 (2012).
27. Davidson, O., Finkelstein, R., Poem, E. & Firstenberg, O. Bright multiplexed source of indistinguishable single photons with tunable GHz-bandwidth at room temperature. *N. J. Phys.* **23**, 073050 (2021).
28. Lasota, M., Filip, R. & Usenko, V. C. Sufficiency of quantum non-Gaussianity for discrete-variable quantum key distribution over noisy channels. *Phys. Rev. A* **96**, 012301 (2017).
29. Rakhubovsky, A. A. & Filip, R. Photon-phonon-photon transfer in optomechanics. *Sci. Rep.* **7**, 1–7 (2017).
30. Niset, J., Fiurášek, J. & Cerf, N. J. No-go theorem for Gaussian quantum error correction. *Phys. Rev. Lett.* **102**, 120501 (2009).
31. Eisert, J., Scheel, S. & Plenio, M. B. Distilling Gaussian states with Gaussian operations is impossible. *Phys. Rev. Lett.* **89**, 137903 (2002).
32. Ghose, S. & Sanders, B. C. Non-Gaussian ancilla states for continuous variable quantum computation via Gaussian maps. *J. Mod. Opt.* **54**, 855–869 (2007).
33. Ohliger, M., Kieling, K. & Eisert, J. Limitations of quantum computing with Gaussian cluster states. *Phys. Rev. A* **82**, 042336 (2010).
34. Lachman, L., Straka, I., Hloušek, J., Ježek, M. & Filip, R. Faithful hierarchy of genuine n-photon quantum non-Gaussian light. *Phys. Rev. Lett.* **123**, 043601 (2019).
35. Sychev, D. V. et al. Enlargement of optical schrödinger's cat states. *Nat. Photonics* **11**, 379–382 (2017).
36. Biagi, N., Costanzo, L. S., Bellini, M. & Zavatta, A. Entangling macroscopic light states by delocalized photon addition. *Phys. Rev. Lett.* **124**, 033604 (2020).
37. Haase, A., Piro, N., Eschner, J. & Mitchell, M. W. Tunable narrowband entangled photon pair source for resonant single-photon single-atom interaction. *Opt. Lett.* **34**, 55–57 (2009).
38. Scholz, M., Koch, L. & Benson, O. Statistics of narrow-band single photons for quantum memories generated by ultrabright cavity-enhanced parametric down-conversion. *Phys. Rev. Lett.* **102**, 063603 (2009).
39. Fekete, J., Rieländer, D., Cristiani, M. & de Riedmatten, H. Ultranarrow-band photon-pair source compatible with solid state quantum memories and telecommunication networks. *Phys. Rev. Lett.* **110**, 220502 (2013).
40. Rambach, M., Nikolova, A., Weinhold, T. J. & White, A. G. Sub-megahertz linewidth single photon source. *APL Photonics* **1**, 096101 (2016).
41. Tsai, P.-J. & Chen, Y.-C. Ultrabright, narrow-band photon-pair source for atomic quantum memories. *Quantum Sci. Technol.* **3**, 034005 (2018).
42. Mottola, R. et al. An efficient, tunable, and robust source of narrow-band photon pairs at the 87 RB d1 line. *Opt. Express* **28**, 3159–3170 (2020).
43. Seri, A. et al. Quantum storage of frequency-multiplexed heralded single photons. *Phys. Rev. Lett.* **123**, 080502 (2019).
44. Moqanaki, A., Massa, F. & Walther, P. Novel single-mode narrow-band photon source of high brightness tuned to cesium d2 line. *APL Photonics* **4**, 090804 (2019).
45. Chen, Q.-F., Shi, B.-S., Feng, M., Zhang, Y.-S. & Guo, G.-C. Non-degenerate non-classical photon pairs in a hot atomic ensemble. *Opt. Express* **16**, 21708–21713 (2008).
46. Willis, R., Becerra, F., Orozco, L. & Rolston, S. Correlated photon pairs generated from a warm atomic ensemble. *Phys. Rev. A* **82**, 053842 (2010).

47. Ding, D.-S., Zhou, Z.-Y., Shi, B.-S., Zou, X.-B. & Guo, G.-C. Generation of non-classical correlated photon pairs via a ladder-type atomic configuration: theory and experiment. *Opt. Express* **20**, 11433–11444 (2012).
48. Shu, C. et al. Subnatural-linewidth biphotons from a doppler-broadened hot atomic vapour cell. *Nat. Commun.* **7**, 1–5 (2016).
49. Lee, Y.-S., Lee, S. M., Kim, H. & Moon, H. S. Highly bright photon-pair generation in Doppler-broadened ladder-type atomic system. *Opt. Express* **24**, 28083–28091 (2016).
50. Zhu, L., Guo, X., Shu, C., Jeong, H. & Du, S. Bright narrowband biphoton generation from a hot rubidium atomic vapor cell. *Appl. Phys. Lett.* **110**, 161101 (2017).
51. Podhora, L., Obšil, P., Straka, I., Ježek, M. & Slodička, L. Nonclassical photon pairs from warm atomic vapor using a single driving laser. *Opt. Express* **25**, 31230–31238 (2017).
52. Zugenmaier, M., Dideriksen, K. B., Sørensen, A. S., Albrecht, B. & Polzik, E. S. Long-lived non-classical correlations towards quantum communication at room temperature. *Commun. Phys.* **1**, 76 (2018).
53. Wang, C. et al. Efficient generation of non-classical photon pairs in a hot atomic ensemble. *Chin. Opt. Lett.* **16**, 082701 (2018).
54. Park, J., Jeong, T., Kim, H. & Moon, H. S. Time-energy entangled photon pairs from doppler-broadened atomic ensemble via collective two-photon coherence. *Phys. Rev. Lett.* **121**, 263601 (2018).
55. Mika, J. & Slodička, L. High nonclassical correlations of large-bandwidth photon pairs generated in warm atomic vapor. *J. Phys. B* **53**, 145501 (2020).
56. Filip, R. & Mišta Jr, L. Detecting quantum states with a positive Wigner function beyond mixtures of Gaussian states. *Phys. Rev. Lett.* **106**, 200401 (2011).
57. Kolchin, P., Du, S., Belthangady, C., Yin, G. Y. & Harris, S. E. Generation of narrow-bandwidth paired photons: use of a single driving laser. *Phys. Rev. Lett.* **97**, 113602 (2006).
58. Mika, J. et al. Generation of ideal thermal light in warm atomic vapor. *N. J. Phys.* **20**, 093002 (2018).
59. Mitchell, M. W., Hancox, C. I. & Chiao, R. Y. Dynamics of atom-mediated photon-photon scattering. *Phys. Rev. A* **62**, 043819 (2000).
60. Park, J., Jeong, T. & Moon, H. S. Temporal intensity correlation of bunched light from a warm atomic vapor with a ladder-type two-photon transition. *Sci. Rep.* **8**, 1–8 (2018).
61. Jeong, T. & Moon, H. S. Temporal-and spectral-property measurements of narrowband photon pairs from warm double-λ-type atomic ensemble. *Opt. Express* **28**, 3985–3994 (2020).
62. Hsu, C.-Y. et al. Generation of sub-MHz and spectrally-bright biphotons from hot atomic vapors with a phase mismatch-free scheme. *Opt. Express* **29**, 4632–4644 (2021).
63. Baek, S.-Y. & Kim, Y.-H. Spectral properties of entangled photons generated via type-i frequency-nondegenerate spontaneous parametric down-conversion. *Phys. Rev. A* **80**, 033814 (2009).
64. Lachman, L. & Filip, R. Robustness of quantum nonclassicality and non-Gaussianity of single-photon states in attenuating channels. *Phys. Rev. A* **88**, 063841 (2013).
65. Podhora, L. et al. Quantum non-Gaussianity of multi-phonon states of a single atom, *Phys. Rev. Lett.* **129**, 013602 (2022).
66. Guo, J. et al. High-performance Raman quantum memory with optimal control in room temperature atoms. *Nat. Commun.* **10**, 148 (2019).
67. Reim, K. F. et al. Single-photon-level quantum memory at room temperature. *Phys. Rev. Lett.* **107**, 053603 (2011).
68. Wolters, J. et al. Simple atomic quantum memory suitable for semiconductor quantum dot single photons. *Phys. Rev. Lett.* **119**, 060502 (2017).
69. Kaczmarek, K. T. et al. High-speed noise-free optical quantum memory. *Phys. Rev. A* **97**, 042316 (2018).
70. Hedges, M. P., Longdell, J. J., Li, Y. & Sellars, M. J. Efficient quantum memory for light. *Nature* **465**, 1052–1056 (2010).
71. Hsiao, Y.-F. et al. Highly efficient coherent optical memory based on electromagnetically induced transparency. *Phys. Rev. Lett.* **120**, 183602 (2018).
72. Vernaz-Gris, P., Huang, K., Cao, M., Sheremet, A. S. & Laurat, J. Highly-efficient quantum memory for polarization qubits in a spatially-multiplexed cold atomic ensemble. *Nat. Commun.* **9**, 1–6 (2018).
73. Wang, Y. et al. Efficient quantum memory for single-photon polarization qubits. *Nat. Photonics* **13**, 346–351 (2019).
74. Li, S. et al. Enhanced cross-phase modulation based on a double electromagnetically induced transparency in a four-level tripod atomic system. *Phys. Rev. Lett.* **101**, 073602 (2008).
75. Liu, Z.-Y. et al. Large cross-phase modulations at the few-photon level. *Phys. Rev. Lett.* **117**, 203601 (2016).
76. Chen, Y.-H. et al. Demonstration of the interaction between two stopped light pulses. *Phys. Rev. Lett.* **108**, 173603 (2012).

ACKNOWLEDGEMENTS

J.M., L.L., and R.F. acknowledge the support of the Czech Science Foundation under the project GA21-13265X. L.S. is grateful for national funding from the MEYS under grant agreement No. 731473 and from the QUANTERA ERA-NET cofund in quantum technologies implemented within the European Union's Horizon 2020 Programme (project PACE-IN, 8C20004). T.L. is grateful for the Palacky University grant IGA-PrF-2022-005.

AUTHOR CONTRIBUTIONS

J.M. and L.S. developed the SFWM source. J.M. realized the main part of the experiment, acquired and processed the measured data. T.L. implemented interferometric measurements of temporal coherence properties. L.L. and R.F. contributed to the evaluation of the QNG states. The project was conceived by L.S. and R.F. All authors discussed the results and contributed to the preparation of the manuscript.

COMPETING INTERESTS

The authors declare no competing interests.

ADDITIONAL INFORMATION

Supplementary information The online version contains supplementary material available at https://doi.org/10.1038/s41534-022-00638-9.

Correspondence and requests for materials should be addressed to Jaromír Mika, Radim Filip or Lukáš Slodička.

Reprints and permission information is available at http://www.nature.com/reprints

Publisher's note Springer Nature remains neutral with regard to jurisdictional claims in published maps and institutional affiliations.